

# Quantum Criticality in Ferromagnetic Single-Electron Transistors

Stefan Kirchner<sup>1</sup>, Lijun Zhu<sup>1,2</sup>, Qimiao Si<sup>1,\*</sup> & D. Natelson<sup>1</sup>

<sup>1</sup>Department of Physics & Astronomy, Rice University, Houston, TX 77251-1892, USA

<sup>2</sup> Department of Physics, University of California, Riverside, CA 92521, USA

## Abstract

Considerable evidence exists for the failure of the traditional theory of quantum critical points (QCPs), pointing to the need to incorporate novel excitations. The destruction of Kondo entanglement and the concomitant critical Kondo effect may underlie these emergent excitations in heavy fermion metals – a prototype system for quantum criticality – but the effect remains poorly understood. Here, we show how ferromagnetic single-electron transistors can be used to study this effect. We theoretically demonstrate a gate-voltage induced quantum phase transition. The critical Kondo effect is manifested in a fractional-power-law dependence of the conductance on temperature ( $T$ ). The AC conductance and thermal noise spectrum have related power-law dependences on frequency ( $\omega$ ) and, in addition, show an  $\omega/T$  scaling. Our results imply that the ferromagnetic nanostructure constitutes a realistic model system to elucidate magnetic quantum criticality that is central to the heavy fermions and other bulk materials with non-Fermi liquid behavior.

A quantum critical point (QCP) occurs at zero temperature as a system changes from one ground state to another, and controls physical properties over a wide region in the phase diagram at finite temperatures [1, 2, 3, 4, 5, 6]. Electrons in condensed matter are traditionally described as a Fermi liquid, a collection of essentially independent particles. Near a QCP, however, electrons are coupled to each other in a singular fashion; how such electron correlations lead to non-Fermi liquid states is an open issue that is central to a variety of strongly correlated systems, including high temperature superconductors and heavy fermion metals [5]. Single-electron devices play a unique role in the study of correlated electronic states, in addition to their potential application to quantum electronics and quantum information processing. The Fermi liquid state has been studied systematically in semiconductor quantum dots and single-molecule transistors [7, 8, 9, 10, 11, 12, 13, 14]. Here, the low-energy excitations of the normal metal leads are electrons near their respective Fermi energies. These itinerant electrons are entangled with the magnetic moment localized on the dot, producing a Kondo

---

\*To whom correspondence should be addressed. Email: qmsi@rice.edu.

resonance. The manifestation of the Kondo resonance in the conductance spectrum was predicted [7, 8] and was subsequently observed in semiconductor quantum dots [9, 10, 11] and in single-molecule transistors [12, 13, 14]. Ingenious proposals and structures [15, 16, 17] have been put forth to model the non-Fermi liquid states associated with the multichannel Kondo systems and the two-impurity Kondo effect [5]. The experimental observation of the non-Fermi liquid states is, however, still lacking, in part because such states of quantum-impurity models are not robust, requiring special symmetries that are difficult to realize [5].

Recently, it has become possible to fabricate single-electron transistors with leads made of ferromagnetic metals [18]. Fig. 1a provides a schematic illustration. The dot, which denotes a quantum-mechanical spin (local moment) of a molecule or that of a semiconductor quantum dot in the Coulomb-blockade regime, is also capacitively coupled to a nonmagnetic gate electrode. Here, we propose this structure as a model system to study how magnetism interplays with the Kondo effect, leading to a QCP with non-Fermi liquid behavior. Our key observation is that the ferromagnetic leads contain not only conduction electrons but also spin waves – collective low-energy excitations arising due to the spontaneously broken spin symmetry of a ferromagnet. We are then led to a description in terms of a Bose-Fermi Kondo model [2, 19, 20, 21, 22], which couples the local moment to both a fermionic bath of conduction electrons and a bosonic one of spin waves.

We focus on the antiparallel (AP) configuration of the magnetizations of the two ferromagnetic leads, and consider symmetric couplings between the dot and the left/right leads. The fermionic bath ( $c_{\mathbf{k}\sigma}$ ) describes a linear combination of the conduction electron bands of the two leads. The bosonic bath contains two components, one each for the two orthogonal spin polarization directions that are perpendicular to the lead magnetizations; each component is a linear combination of the corresponding spin waves in the two leads. We note on a number of features of the resulting Bose-Fermi Kondo model [see Eq. (9) of the Formal Details section] specific to the system. First, while the energy bands of the two spin components of the conduction electrons in each metallic lead is (Zeeman) split by the magnetization, the linear combination that forms the fermionic bath contains no Zeeman splitting (Refs. [23, 24], and references therein) as can be readily seen from Fig. 1b. Second, in addition to fringing fields from the ferromagnetic leads, an effective local magnetic field ( $h_{\text{loc}}$ ) for the local moment is usually generated due to dot-lead exchange coupling. In our AP case, however, the contributions from the two leads compensate with each other and  $h_{\text{loc}}$  vanishes. Third, the two-component nature of the bosonic bath means that our model has an easy-plane spin anisotropy. Finally, the dispersion of the ferromagnetic spin waves ( $\omega_{\mathbf{q}}$ ) is such that the spectral density of the bosonic bath has a square-root dependence on the frequency,

$$\sum_{\mathbf{q}} \delta(\omega - \omega_{\mathbf{q}}) \propto \sqrt{\omega}, \quad (1)$$

for  $0 < \omega < \Lambda$ , the cutoff frequency below which spin waves exist (*cf.*

Fig. 1c). The sub-linear dependence on frequency is commonly referred to as “sub-ohmic” dissipation. We note that the gap of spin waves in real ferromagnets is non-zero; its effect will be discussed shortly.

We find that a quantum phase transition can be induced by varying the gate voltage,  $V_g$ . This voltage determines  $\Delta$ , the valence-fluctuation energy cost of the dot:  $\Delta = \Delta_0 - cV_g$ , where  $\Delta_0$  is the corresponding energy cost in the absence of the gate voltage and the proportionality factor  $c = eC_{\text{gate}}/C_{\text{tot}}$  is determined by the gate and total capacitances,  $C_{\text{gate}}$  and  $C_{\text{tot}}$ , respectively. The parameter  $\Delta$  in turn determines the strength of the interactions between the local moment and the bosonic and fermionic baths. The local-moment regime arises when  $\Delta \gg \Gamma \equiv \pi\rho_0 t^2$ , the non-interacting resonance width; here,  $t$  is the dot-lead hybridization matrix and  $\rho_0$  the fermion density of states at the chemical potential. The resulting Bose-Fermi Kondo model is given in Eq. (9) of the Formal Details section. The Kondo exchange coupling with the fermions, and the bare Kondo scale (at  $g = 0$ ), have the standard forms:  $J \sim \Gamma/\rho_0\Delta$  and  $T_K^0 \sim (1/\rho_0)\exp(-\pi\Delta/\Gamma)$ , respectively. The coupling with the bosonic bath is found (see the Formal Details section) to be  $g \sim \Gamma/(\rho_0\Delta)^2$ . Hence, the ratio  $g/T_K^0$  is exponentially large, and it decreases as  $\Delta$  is reduced. When  $\Delta$  becomes comparable to  $\Gamma$ , the system reaches the mixed-valence regime, and  $g/T_K^0$  becomes of order unity. Changing  $V_g$  then takes the system through second-order quantum phase transition (Fig. 1d).

More specifically, for gate voltages such that the system (dot + leads) is either in the mixed valence regime or in the local-moment regime but with moderate ratios of  $\Delta/\Gamma$ , the usual Kondo effect takes place. At low temperatures, the system is in a Fermi liquid ground state. As  $\Delta$  is increased by varying  $V_g$ , interactions with the spin waves destroy the Kondo effect. Kondo resonances no longer form, and the system is in a non-Fermi liquid ground state. In between the system passes through a QCP, which is also a non-Fermi liquid. These phases and the phase transition are expressed in terms of the renormalization group (RG) flows and RG fixed points in Fig. 1d. At relatively small  $g/T_K^0$ , the RG flow is towards the Kondo fixed point. For sufficiently large  $g$ , the flow is instead towards a fixed point located on the  $J = 0$  axis (the horizontal line of Fig. 1d) where the local moment is completely decoupled from the fermions but is still strongly fluctuating [25] through the coupling to the spin waves. We will call this phase in the entire  $g > g_c$  region a “critical local-moment phase”. In between, the system passes through  $g = g_c$  where the RG flow is towards a quantum-critical fixed point. Here, the local moment fluctuates in a critical fashion (at time scales beyond the short-time cutoff,  $\hbar/T_K^0$ ) and the electronic excitations have a non-Fermi liquid form. The sub-ohmic nature of the dissipative bosonic bath [Eq. (1)] is necessary for the existence of quantum criticality.

## Results and Discussion

To systematically study the transport properties across the quantum phase transition, we apply a dynamical large-N approach [27, 28, 29] to the Bose-

Fermi Kondo model (see the Formal Details section). We first consider the single-electron spectral function on the dot, expressed in terms of the scattering T-matrix. The results are shown in Fig. 2. Since the universal properties are insensitive to the way the quantum-critical regime is accessed, we have, for convenience, chosen to work with fixed  $T_K^0$  and varying  $g$ . The different curves correspond to different ratios of  $g/T_K^0$  and, correspondingly, different values of the gate-voltage  $V_g$ . The spectral weight of the Kondo resonance is seen to decrease as  $g$  increases, and vanishes continuously when  $g$  reaches  $g_c$ . At the QCP, the Kondo screening is critical: a Kondo resonance is no longer fully developed but vestiges of it remain. For  $g > g_c$ , the Kondo effect is completely destroyed: the spectral density vanishes at  $\omega = 0$ . At finite energies, however, the spectral density is still finite reflecting on a finite effective (scale-dependent, *or* renormalized) Kondo coupling.

The linear-response DC conductance ( $G$ ) directly manifests the critical nature of the Kondo effect. Its temperature dependence is given in Fig. 3. On the Kondo side ( $g < g_c$ ), the conductance increases as the temperature is lowered, reflecting the development of a Kondo resonance [7, 8]. Inside the critical local-moment phase ( $g > g_c$ ), the conductance vanishes in a power-law form as temperature goes to zero. It vanishes at  $T = 0$  since Kondo screening has been completely destroyed. At finite temperatures, charge transport can still occur because of the finite effective Kondo coupling at non-zero energies. Hence, the way the conductance goes to zero characterizes the critical behavior of the Kondo coupling at the critical local-moment fixed point. At the QCP ( $g = g_c$ ), the conductance behaves in a way intermediate between the two sides. The zero-temperature conductance is finite, but is reduced from its counterpart on the Kondo side. The temperature-dependent part has a power-law form that is distinct from both the local-moment and Kondo sides, characterizing the critical exponents unique to the QCP.

To understand the detailed temperature dependences, we have analytically determined the zero-temperature T-matrix. At the QCP ( $g = g_c$ ), its imaginary part is  $\mathcal{T}''(\omega + i0^+, T = 0) = a + b|\omega|^{1/4}$ . On the local-moment side ( $g > g_c$ ), the asymptotic low-energy behavior is  $\mathcal{T}''(\omega + i0^+, T = 0) = c|\omega|^{1/2}$ . The exponents here reflect the critical exponents of the QCP and the critical local moment phase with a dissipative spectrum given in Eq. (1). The results suggest that the linear response DC conductance is, at the QCP,

$$G(T) = A + BT^{1/4}, \quad (2)$$

and, inside the critical local-moment phase ( $g > g_c$ ),

$$G(T) = CT^{1/2}. \quad (3)$$

Indeed, these fractional-power-law forms fit the numerical results shown in Fig. 3. The success of this fitting suggests that the T-matrix satisfies an  $\omega/T$  scaling. This is verified by the scaling plots shown in Fig. 4a for  $g = g_c$  and in Fig. 4b for  $g > g_c$ .

AC transport and noise properties provide the means to probe the  $\omega/T$

scaling. At the QCP, the real part of the AC conductance is

$$G'(\omega, T) = \mathcal{G}_{c0}(\omega/T) + \omega^{1/4}\mathcal{G}_{c1}(\omega/T), \quad (4)$$

whereas, inside the local-moment phase ( $g > g_c$ ),

$$G'(\omega, T) = \omega^{1/2}\mathcal{G}_b(\omega/T). \quad (5)$$

Here,  $\mathcal{G}_{c0}$ ,  $\mathcal{G}_{c1}$  and  $\mathcal{G}_b$  are scaling functions. The thermal current fluctuations (Johnson noise) spectrum,  $S(\omega)$ , is simply Eqs. (4,5) multiplied by  $2\hbar\omega[1 + n_B(\omega)]$ , where the Bose factor  $n_B(\omega) \equiv 1/[e^{\hbar\omega/k_B T} - 1]$ .  $S(\omega)/\omega$ , too, satisfies  $\omega/T$  scaling at the QCP and inside the critical local-moment phase.

We turn next to the feasibility of the experimental measurements. The non-Fermi liquid behavior we have derived applies to the scaling regime, the region in which universal properties arise. We have so far assumed a spin-wave spectrum that is gapless. Real ferromagnets contain interactions (such as spin-orbit coupling) that break spin-rotational symmetry, which will cut off the scaling regime at low energies. The bulk spin-anisotropic interaction results in a spin wave gap of about 0.25 K for Ni films [31] and even smaller values in the case of permalloys. The surface spin-anisotropic interactions yield a finite de-pinning energy which, however, is negligibly small (of the sub mK range; see the Formal Details section). The upper cutoff energy of the scaling regime is given by the Kondo scale,  $T_K^0$ , which, for single-molecular transistors, can be of the order of 50 – 100 K (Refs. [14, 32]). Hence, we can expect more than two decades of both temperature and frequency over which the non-Fermi liquid behavior occurs. To study the AC noise spectrum, the frequencies needed fall in the range of about a few gigahertz to a terahertz. Much of this frequency range is already feasible experimentally: noise measurements up to 90 gigahertz have been reported [33].

We have also assumed symmetric couplings of the dot to the two leads, which ensure a zero local effective magnetic field for the local moment due to exchange ( $h_{loc} = 0$ ). [The fringing fields from the ferromagnetic leads are expected to be small ( $\ll 0.6\text{K}$  for Ni) [18].] Significantly different left/right couplings will yield a finite  $h_{loc}$  (which, on the Kondo side, in turn results in a splitting of the Kondo resonances even in the AP configuration [18, 23, 24]). Some of the single-molecule transistors reported in Ref. [18] indeed have approximately symmetric couplings, as evidenced by the smallness of the splitting in the Kondo peaks. Even if it is nonzero,  $h_{loc}$  can be compensated by an external local magnetic field [23]. The latter can be generated by dc currents through nearby conductors, as in magnetic random access memory applications [34].

So far, we have considered ferromagnetic metallic leads. A variation is to use metallic leads which are paramagnetic, but are nearly ferromagnetic. The absence of static ordering implies that the local effective field (from dot-lead exchange) vanishes under all circumstances. Spin waves are no longer sharply defined; they do, nonetheless, appear in the form of paramagnons,

which provide a dissipative bosonic bath with a fluctuation spectrum similar to that of Eq. (1), but with an exponent  $1/3$ , instead of  $1/2$ . This is still sub-ohmic, so with appropriate modifications to the fractional exponent and scaling functions, essentially all our results will still apply. (The almost magnetic nature of the leads here can generate multi-channels of effective conduction electrons [35, 36], which can influence the finite temperature properties on the Kondo side. This effect, however, is not expected to modify the quantum critical behavior.) For instance, the conductance exponent at  $g = g_c$  is now  $1/3$  (instead of  $1/4$ ), and that for  $g > g_c$  becomes  $2/3$  (instead of  $1/2$ ). Palladium would be one candidate material in this category.

Our results are insensitive to the presence or absence of particle-hole symmetry. In addition, there is no need to achieve multiple channels of fermionic couplings. These make the non-Fermi liquid behavior of a ferromagnetic single-electron transistor more robust than that of either the multi-channel or multi-impurity Kondo systems. There is a simple reason behind this robustness. The phases of the system we have discussed – the Kondo phase on the one hand and the critical local-moment phase on the other – are genuinely distinct and must be separated by a quantum phase transition. Since the transition is second order, a distinctive QCP must arise and quantum criticality in turn makes the system a non-Fermi liquid. In the multi-channel or multi-impurity Kondo systems [5], however, all the stable phases are Fermi liquids, making special symmetries – channel degeneracy or particle-hole symmetry – necessary to reach any non-Fermi liquid state.

It is instructive to discuss the broader implications of our results. Orthodox theory of any QCP [4, 6] describes it in terms of order-parameter fluctuations and maps it to a classical counterpart in elevated dimensions. For the Bose-Fermi Kondo model with a bosonic fluctuation spectrum given by Eq. (1), the corresponding critical point is non-interacting [27, 37, 38]. On the other hand, the  $\omega/T$  scaling implies [4] that the critical point we are dealing with is a fully interacting one. A further support for the interacting nature of the QCP comes from Fig. 4a. It is seen that the T-matrix at the limit of zero temperature and  $\omega \rightarrow 0$  [corresponding to  $\omega/T \gg 1$  and yielding  $\mathcal{G}_{c0}(\infty)$  – *cf.* Eq. (4)] is different from that at the limit of  $\omega = 0$  and  $T \rightarrow 0$  [so that  $\omega/T \ll 1$ , giving rise to  $\mathcal{G}_{c0}(0)$ ]. This is in contrast to non-interacting critical points of quantum impurity models in which the two limits are believed to be interchangeable [39]. An experimental observation of either  $\omega/T$  scaling, or  $\mathcal{G}_{c0}(\infty) \neq \mathcal{G}_{c0}(0)$ , would provide a direct signature of the inherent quantum nature of the QCP.

In addition to their intrinsic interest, our results will establish how the Kondo effect influences quantum criticality. The latter not only is directly relevant to the quantum-critical heavy fermions [1, 2, 3], whose properties strongly deviate from the expectations of the order-parameter-fluctuation picture, but also illustrates the central role of quantum entanglement effects – beyond the fluctuations of order parameter – in quantum criticality in

general.

## Conclusions

To summarize, we propose the ferromagnetic single-electron transistor as a model system to study non-Fermi liquid states and quantum criticality. We have shown that the quantum critical point is robust theoretically and feasible in experimental implementation. Finally, our results imply that the system, readily measurable beyond the equilibrium regime, will serve as an ideal setting for the much-needed explorations of the non-equilibrium properties at quantum criticality. All these features make it a tunable spintronic system to study issues that are important to a broad array of strongly correlated electron materials.

## Formal Details

**Derivation of the Bose-Fermi Kondo model.** Consider the regime where the dot has an odd number of electrons and the valence-fluctuation energy  $\Delta$  is large compared to the resonance width  $\Gamma$ . At temperatures well below  $\Delta/k_B$ , valence fluctuations can occur only virtually and the dot is effectively a localized moment. Hybridization processes between the dot and electrodes give rise to an antiferromagnetic coupling between this moment and the spins of the low-energy conduction electrons in the lead metal. The conduction-electron spin in a direction perpendicular to the ordered moments of the ferromagnets is a linear combination of the transverse part of the triplet quasiparticle-hole excitations and the spin waves. So we expect the local moment to be coupled not only to the spins of the quasiparticles but also to the spin waves. In order to determine the specific value of the bosonic coupling constant, we go beyond these general arguments and carry out a generalized Schrieffer-Wolff transformation followed by a projection ( $\mathcal{P}$ ) onto the local-moment subspace:

$$\mathcal{H}_{\text{bfk}} = \mathcal{P} e^S (H_0 + H_{\text{lead}} + H_{\text{hyb}}) e^{-S} \mathcal{P}, \quad (6)$$

where  $H_0$  is the charge-conserving part of the dot Hamiltonian. The generator of the canonical transformation ( $S$ ) follows from the requirement that  $[H_0 + H_{\text{lead}}, S] = H_{\text{hyb}}$ , and can be formally expressed as [40],

$$S = (L_{\text{lead}} + L_0)^{-1} H_{\text{hyb}}, \quad (7)$$

where the Liouville operators are defined as  $L_x A = [H_x, A]$ . We model the ferromagnetic metal of a lead in terms of a one-band Hamiltonian,  $H_{\text{lead}} = \sum_i H_{\text{kin},i} - \frac{2u}{3} \sum_{\mathbf{r},i} (\mathbf{s}_i(\mathbf{r}))^2$ , where  $H_{\text{kin},i} = \sum_{\mathbf{k},\sigma} \epsilon_{\mathbf{k}} c_{\mathbf{k}\sigma i}^\dagger c_{\mathbf{k}\sigma i}$ , with  $i = L, R$  being the lead index. The interaction term is decoupled in terms of the vector boson field  $\vec{\phi}$  as follows,

$$\begin{aligned} H_{\text{lead}} &= \sum_i H_{\text{kin},i} + \sum_{\mathbf{r},i} \left[ \frac{1}{2} u \vec{\phi}_i^\dagger(\mathbf{r}) \cdot \vec{\phi}_i(\mathbf{r}) \right. \\ &\quad \left. + \lambda [\phi_i(\mathbf{r}) + \vec{\phi}_i^\dagger(\mathbf{r})] \cdot \mathbf{s}_i(\mathbf{r}) \right], \end{aligned} \quad (8)$$

where  $\lambda = \sqrt{2/3}u$ . Within the ferromagnetic-metal phase, the  $z$ -component  $\phi_{z,i}$  acquires a static value,  $m_i$ , and the transverse components  $\phi_{\beta,i}$ ,  $\beta = x, y$ , describe the spin waves. Inserting Eqs. (7,8) in Eq. (6) leads to a Bose-Fermi Kondo model,

$$\begin{aligned} \mathcal{H}_{\text{bfk}} = & J \sum_i \mathbf{S} \cdot \mathbf{s}_i + \sum_{\mathbf{k}, i, \sigma} \tilde{\epsilon}_{\mathbf{k}\sigma i} c_{\mathbf{k}\sigma i}^\dagger c_{\mathbf{k}\sigma i} + gS_z \sum_i m_i \\ & + gS_\beta \sum_{\beta, \mathbf{q}, i} (\phi_{\beta, \mathbf{q}, i} + \phi_{\beta, \mathbf{q}, i}^\dagger) + \sum_{\beta, \mathbf{q}, i} \omega_{\mathbf{q}} \phi_{\beta, \mathbf{q}, i}^\dagger \phi_{\beta, \mathbf{q}, i}, \end{aligned} \quad (9)$$

with the coupling constant  $g \sim ut^2/\Delta^2$  which gives rise to the expression for  $g$  stated earlier once we recognize that, in itinerant ferromagnets,  $\rho_0 u \sim 1$ . The conduction electron dispersion in each lead is Zeeman split:  $\tilde{\epsilon}_{\mathbf{k}\sigma i} = \epsilon_{\mathbf{k}} + \lambda m_i \sigma$ . However, only one linear combination of the conduction electrons from the two leads is coupled to the dot spin [7, 8]:  $c_{\mathbf{k}\sigma} = (c_{\mathbf{k}\sigma L} + c_{\mathbf{k}\sigma R})/\sqrt{2}$ . The energy dispersion for this linear combination is spin-independent, and will be denoted as  $E_{\mathbf{k}}$ . A similar linear combination arises for the spin waves from the two leads:  $\Phi = (\phi_L + \phi_R)/\sqrt{2}$ . The local effective field,  $h_{\text{loc}} = g \sum_i m_i$ , vanishes in the AP case ( $m_L = -m_R$ ). The Hamiltonian (9) has an easy-plane anisotropy. Taking advantage of the observation [26, 27] that the scaling properties of both the quantum critical point and the critical local-moment phase in this case are similar to those of its SU(2) and SU(N) counterparts, we will generalize the local moment to a form with SU(N) symmetry, and the conduction electrons to a form with SU(N)  $\times$  SU(N/2) symmetry [28, 29]. After a rescaling of the Kondo coupling to order  $1/N$ , and the coupling to the spin waves to order  $1/\sqrt{N}$ , we arrive at the Hamiltonian:

$$\begin{aligned} \mathcal{H}_{\text{BFK}} = & (J/N) \sum_{\alpha} \mathbf{S} \cdot \mathbf{s}_{\alpha} + \sum_{\mathbf{k}, \alpha, \sigma} E_{\mathbf{k}} c_{\mathbf{k}\alpha\sigma}^\dagger c_{\mathbf{k}\alpha\sigma} \\ & + (g/\sqrt{N}) \mathbf{S} \cdot \Phi + \sum_{\mathbf{q}} \omega_{\mathbf{q}} \Phi_{\mathbf{q}}^\dagger \cdot \Phi_{\mathbf{q}}. \end{aligned} \quad (10)$$

Here,  $\mathbf{S}$ ,  $c_{\mathbf{k}\alpha\sigma}$ , and  $\Phi_{\mathbf{q}}$  denote the local moment, fermionic bath and bosonic bath, respectively,  $\Phi = \sum_{\mathbf{q}} (\Phi_{\mathbf{q}} + \Phi_{\mathbf{q}}^\dagger)$  and  $\mathbf{s}_{\alpha} = (1/2) \sum_{\mathbf{k}\sigma, \mathbf{k}'\sigma'} c_{\mathbf{k}\alpha\sigma}^\dagger \vec{\tau}_{\sigma, \sigma'} c_{\mathbf{k}'\alpha\sigma'}$  where  $\vec{\tau}$  is the vector of Pauli matrices.  $\sigma = 1, \dots, N$  labels spin indices and  $\alpha = 1, \dots, N/2$  the channel indices for conduction electrons.

The spin-wave spectrum determines the dissipative bosonic bath spectrum. We end up with Eq. (1) using the spin-wave dispersion  $\omega_{\mathbf{q}} = \rho_s q^2$ , where  $\rho_s$  is the spin-wave stiffness.

**Dynamical large-N method.** The dynamical saddle-point equations for the large- $N$  limit of the Bose-Fermi Kondo Hamiltonian have been described in Ref. [27]. In addition to allowing a controlled solution in general, this limit allows us to calculate the conduction electron T-matrix. The saddle-point equations are expressed in terms of  $G_f(\tau)$  and  $G_B(\tau)$ , the propagators for the slave- $f$ -fermion of the dot spin and for the  $B$ -field representing the  $f^\dagger c$  combination [27, 28, 29], respectively. Once these quantities are determined, the T-matrix is given by the Fourier transform of  $\mathcal{T}(\tau) = -\frac{1}{N} G_B(-\tau) G_f(\tau)$ . The large  $N$  limit for the Kondo phase ( $g < g_c$ ) is described by the fixed



point at  $g = 0$ , which is a multi-channel fixed-point [28, 29]. For the critical local moment phase ( $g > g_c$ ) and the QCP ( $g = g_c$ ), on the other hand, both the large  $N$  and the  $N = 2$  cases describe non-Fermi liquid states and the two cases have similar critical behaviors [26, 27].

At  $T = 0$ , the large- $N$  limit is solved analytically, by making the scaling ansatz for both the leading and sub-leading terms,

$$G_f(\tau) = \frac{A_1}{\tau^{\alpha_1}} + \frac{A_2}{\tau^{\alpha_2}}; \quad G_B(\tau) = \frac{B_1}{\tau^{\beta_1}} + \frac{B_2}{\tau^{\beta_2}}, \quad (11)$$

and inserting these into the saddle-point equations. Consider first the leading order. For the critical local-moment phase,  $\alpha_1 = 1/4$  and  $\beta_1 = 5/4$ . As a result,  $\mathcal{T}(\tau) \sim 1/\tau^{3/2}$ , corresponding to an  $\omega^{1/2}$  dependence. [In the more general case with  $\omega^{1-\epsilon}$  replacing  $\sqrt{\omega}$  in Eq. (1), the result is  $\omega^\epsilon$ .] For the QCP ( $g = g_c$ ),  $\alpha_1 = 1/4$  and  $\beta_1 = 3/4$ , yielding  $\mathcal{T}(\tau) \sim 1/\tau$ , corresponding to a constant  $\mathcal{T}''(\omega + i0^+)$  [the critical exponent at the leading order (being equal to 1), though neither the critical amplitude (the constant  $a$  given below) nor the finite-temperature behavior (Fig. 4a), was anticipated by the general argument of Ref. [30]]. The  $\omega$ -dependence comes from the subleading terms of  $G_f(\tau)$  and  $G_B(\tau)$ . We find  $\alpha_2 = 1/2$  and  $\beta_2 = 1$ , making the dominant subleading contribution to  $\mathcal{T}(\tau)$  to be  $1/\tau^{5/4}$  which, in turn, corresponds to an  $\omega^{1/4}$  dependence. (For general  $\epsilon$ , this becomes  $\omega^{\epsilon/2}$ .) The final results, for  $g = g_c$  and  $g > g_c$ , are given in the Results and Discussion section, just before Eq. (2), with the numerical factors  $a = \tan(\pi/8)/(8N\rho_0)$ ,  $b = \pi[5 \tan(\pi/8)]^{1/2}/[N\rho_0 K_0 g_c \Gamma^3(1/4)]$ , and  $c = (1/8)\Gamma(5/4)[3 \tan(\pi/8)/2]^{1/2} J/[N K_0 g \Lambda^{1/4}]$ . Here,  $\Gamma(x)$  is the gamma function and  $K_0 = [\Gamma(3/2)/4\pi^2 \rho_s^{3/2}]^{1/2}$  is related to the proportionality factor on the right hand side of Eq. (1).

At finite temperatures, the saddle-point equations in the large- $N$  limit are solved numerically in terms of real frequencies [27]. To check the robustness of our results with respect to particle-hole symmetry breaking, we have also solved the extension of the above saddle-point equations to the Bose-Fermi Anderson model in the local-moment regime without particle-hole symmetry (setting  $N = 2$ ):

$$\begin{aligned} H_{\text{bfam}} &= \sum_{\mathbf{k}, \sigma} E_{\mathbf{k}} c_{\mathbf{k}\sigma}^\dagger c_{\mathbf{k}\sigma} + \varepsilon_d \sum_{\sigma} d_{\sigma}^\dagger d_{\sigma} + U n_{d\uparrow} n_{d\downarrow} \\ &+ t \sum_{\mathbf{k}, \sigma} \left( c_{\mathbf{k}\sigma}^\dagger d_{\sigma} + \text{h.c.} \right) + g \mathbf{S}_d \cdot \mathbf{\Phi} \\ &+ \sum_{\mathbf{q}} \omega_{\mathbf{q}} \mathbf{\Phi}_{\mathbf{q}}^\dagger \cdot \mathbf{\Phi}_{\mathbf{q}}, \end{aligned} \quad (12)$$

with  $\mathbf{S}_d = (1/2) \sum_{\sigma, \sigma'} d_{\sigma}^\dagger \vec{\tau}_{\sigma, \sigma'} d_{\sigma'}$ , and  $\varepsilon_d \neq -U/2$ . The scaling behavior is found to be the same as that of either the numerical results in the large  $N$  limit we have considered, which has a particle-hole symmetry, or (where a comparison can be made) the analytical results in the same limit.

**Calculation of the transport quantities.** The linear-response DC con-

ductance is

$$\begin{aligned}
G &= \lim_{V \rightarrow 0} \frac{dI}{dV} \\
&= \frac{e^2}{\hbar} N\Gamma \int_{-\infty}^{\infty} d\epsilon \frac{1}{\pi} \mathcal{T}''(\epsilon + i0^+) \left[ -\frac{\partial f(\epsilon)}{\partial \epsilon} \right], \quad (13)
\end{aligned}$$

where  $f(\epsilon)$  is the Fermi-Dirac distribution function. Likewise, the real part of the linear-response AC conductance (the current response to an oscillating bias voltage) can also be related to the scattering T-matrix [41, 42] under the condition of vanishing charge accumulation:

$$\begin{aligned}
G'(\omega) &= \frac{e^2}{2\hbar} N\Gamma \int_{-\infty}^{\infty} d\epsilon \frac{1}{\pi} \mathcal{T}''(\epsilon + i0^+) \times \\
&\quad \left[ f(\epsilon - \hbar\omega) - f(\epsilon + \hbar\omega) \right] / (\hbar\omega). \quad (14)
\end{aligned}$$

The thermal current-fluctuation noise spectrum is simply related to  $G'(\omega)$  through the fluctuation-dissipation theorem. The result is given in Eqs. (4,5), with the following limiting values:  $\mathcal{G}_{c0}(x \rightarrow \infty) = 2aG_0\Gamma/\hbar$ ,  $\mathcal{G}_{c1}(x \rightarrow \infty) = 8bG_0\Gamma/(5\hbar)$ , and  $\mathcal{G}_b(x \rightarrow \infty) = 8cG_0\Gamma/(5\hbar)$ .

**De-pinning energy of spin waves at the surface.** The form of the coupling between the local moment and spin waves, given in the third term on the right hand side of Eq. (9), has been derived in the absence of any surface spin-anisotropic interaction. The latter introduces a pinning of the spin waves of sufficiently long wavelengths [43]. Below the pinning wavevector,  $q < q_{\text{pin}}$ , the wavefunction at the surface is linearly [43, 44] proportional to  $q$ ; in turn, the coupling constant between  $S_\beta$  and  $\phi_{\beta,\mathbf{q},i}$  is proportional to  $q$ , changing the spectrum of the dissipative bath from Eq. (1) to  $\sim \omega^{3/2}$ . From the known result [43, 44]  $q_{\text{pin}}a \approx E_{\text{sa}}/E_{\text{ex}}$ , where  $a$  is the lattice constant and  $E_{\text{sa}}$  and  $E_{\text{ex}}$  are respectively the surface anisotropic and bulk isotropic exchange energies, we can estimate the corresponding pinning energy scale  $E_{\text{pin}} \approx E_{\text{ex}}(q_{\text{pin}}a)^2 = E_{\text{sa}}^2/E_{\text{ex}}$ . (Here, we have used the mean-field expression  $\rho_s \approx E_{\text{ex}}a^2$ .) Being smaller than  $E_{\text{sa}}$  by a factor  $E_{\text{sa}}/E_{\text{ex}}$ , the pinning energy is expected to be rather small. For Fe-Co films, for instance,  $E_{\text{sa}} \sim 1$  K (corresponding to a typical surface anisotropy [45] of the order  $0.1$  erg/cm<sup>2</sup>) and  $E_{\text{ex}} > \sim 1000$  K (based on the Curie temperature), giving rise to an  $E_{\text{pin}} < 1$  mK.

**Acknowledgments** We would like to thank E. Abrahams, K. Ingersent, C. M. Varma, and G. Zaránd for useful discussions. This work has been supported by DFG (SK), Robert A. Welch Foundation, NSF Grant No. DMR-0424125 (SK, LZ, & QS), the Alfred P. Sloan Foundation, the David and Lucille Packard Foundation and NSF Grant No. DMR-0347253 (DN).

## References

- [1] Coleman, P. & Schofield, A. J. (2005) *Nature* **433**, 226–229.

- [2] Si, Q., Rabello, S., Ingersent, K., & Smith, J. (2001) *Nature* **413**, 804–808.
- [3] Paschen, S., Lühmann, T., Wirth, S., Gegenwart, P., Trovarelli, O., Geibel, C., Steglich, F., Coleman, P., & Si, Q. (2004) *Nature* **432**, 881–885.
- [4] Sachdev, S. (1999) *Quantum Phase Transitions*. (Cambridge Univ. Press, Cambridge).
- [5] Varma, C. M., Nussinov, Z., & van Saarloos, W. (2002) *Phys. Rep.* **361**, 267–417.
- [6] Hertz, J. (1976) *Phys. Rev. B* **14**, 1165–1184.
- [7] Glazman, L. I. & Raikh, M. E. (1988) *JETP Lett.* **47**, 452–455.
- [8] Ng, T. & Lee, P. (1988) *Phys. Rev. Lett.* **61**, 1768–1771.
- [9] Goldhaber-Gordon, D., Shtrikman, H., Mahalu, D., Abusch-Magder, D., Meirav, U., & Kastner, M. A. (1998) *Nature* **391**, 156 – 159.
- [10] Cronenwett, S., Oosterkamp, T., & Kouwenhoven, L. (1998) *Science* **281**, 540–544.
- [11] Schmid, J., Weis, J., Eberl, K., & v. Klitzing, K. (1998) *Physica B* **258**, 182–185.
- [12] Park, J., Pasupathy, A. N., Goldsmith, J. I., Chang, C., Yaish, Y., Petta, J. R., Rinkoski, M., Sethna, J. P., Abruna, H. D., McEuen, P. M., & Ralph, D. C. (2002) *Nature* **417**, 722–725.
- [13] Liang, W. J., Shores, M. P., Bockrath, M., Long, J. R., & Park, H. (2002) *Nature* **417**, 725–729.
- [14] Yu, L. H. & Natelson, D. (2004) *Nano Letters* **4**, 79–83.
- [15] Oreg, Y. & Goldhaber-Gordon, D. (2003) *Phys. Rev. Lett.* **90**, 136602.
- [16] Pustilnik, M., Borda, L., Glazman, L. I., & von Delft, J. (2004) *Phys. Rev. B* **69**, 115316.
- [17] Craig, N. J., Taylor, J. M., Lester, E. A., Marcus, C. M., Hanson, M. P., & Gossard, A. C. (2004) *Science* **304**, 565–567.
- [18] Pasupathy, A. N., Bialczak, R. C., Martinek, J., Grose, J. E., Donev, L. A. K., McEuen, P. L., & Ralph, D. C. (2004) *Science* **306**, 86–89.
- [19] Smith, J. L. & Si, Q. (1999) *Europhys. Lett.* **45**, 228–234.
- [20] Sengupta, A. M. (2000) *Phys. Rev. B* **61**, 4041–4043.
- [21] Zhu, L. & Si, Q. (2002) *Phys. Rev. B* **66**, 024426.
- [22] Zaránd, G. & Demler, E. (2002) *Phys. Rev. B* **66**, 024427.

- [23] Martinek, J., Sindel, M., Borda, L., Barnas, J., König, J., Schön, G., & von Delft, J. (2003) *Phys. Rev. Lett.* **91**, 247202.
- [24] Choi, M. S., Sanchez, D., & Lopez, R. (2004) *Phys. Rev. Lett.* **92**, 056601.
- [25] Sachdev, S. & Ye, J. (1993) *Phys. Rev. Lett.* **70**, 3339–3342.
- [26] Kirchner, S., Zhu, L., & Si, Q. (2005) *Physica B* **359-361**, 83.
- [27] Zhu, L., Kirchner, S., Si, Q., & Georges, A. (2004) *Phys. Rev. Lett.* **93**, 267201.
- [28] Parcollet, O. & Georges, A. (1998) *Phys. Rev. B* **58**, 3794.
- [29] Cox, D. & Ruckenstein, A. (1993) *Phys. Rev. Lett.* **71**, 1613–1616.
- [30] Vojta, M. & Kiréan, M. (2003) *Phys. Rev. Lett.* **90**, 157203.
- [31] van Kampen, M., Jozsa, C., Kohlhepp, J. T., LeClair, P., Lagae, L., de Jonge, W. J. M., & Koopmans, B. (2002) *Phys. Rev. Lett.* **88**, 227201.
- [32] Yu, L., Keane, Z., Ciszek, J., Cheng, L., Tour, J., Baruah, T., Pederson, M., & Natelson, D. (2005). cond-mat/0505683.
- [33] Deblock, R., Onac, E., Gurevich, L., & Kouwenhoven, L. P. (2003) *Science* **301**, 203–206.
- [34] Engel, B., Rizzo, N., Janesky, J., Slaughter, J., Dave, R., DeHerrera, M., Durlam, M., & Tehrani, S. (2002) *IEEE Transactions on Nanotechnology* **1**, 32–38.
- [35] Maebashi, H., Miyake, K., & Varma, C. M. (2002) *Phys. Rev. Lett.* **88**, 226403.
- [36] Larkin, A. I. & Melnikov, V. I. (1972) *Sov. Phys. JETP* **34**, 656–661.
- [37] Vojta, M., Tong, N.-H., & Bulla, R. (2005) *Phys. Rev. Lett.* **94**, 070604.
- [38] Glossop, M. T. & Ingersent, K. (2005) *Phys. Rev. Lett.* **95**, 067202.
- [39] Damle, K. & Sachdev, S. (1997) *Phys. Rev. B* **56**, 8714–8733.
- [40] Schork, T. & Fulde, P. (1994) *Phys. Rev. B* **50**, 1345–1350.
- [41] Sindel, M., Hofstetter, W., von Delft, J., & Kindermann, M. (2005) *Phys. Rev. Lett.* **94**, 196602.
- [42] Büttiker, M., Pretre, A., & Thomas, H. (1993) *Phys. Rev. Lett.* **70**, 4114–4117.
- [43] Kittel, C. (1958) *Phys. Rev.* **110**, 1295–1297.
- [44] Pincus, P. (1960) *Phys. Rev.* **118**, 658–664.
- [45] Schreiber, F. & Frait, Z. (1996) *Phys. Rev. B* **54**, 6473–6480.

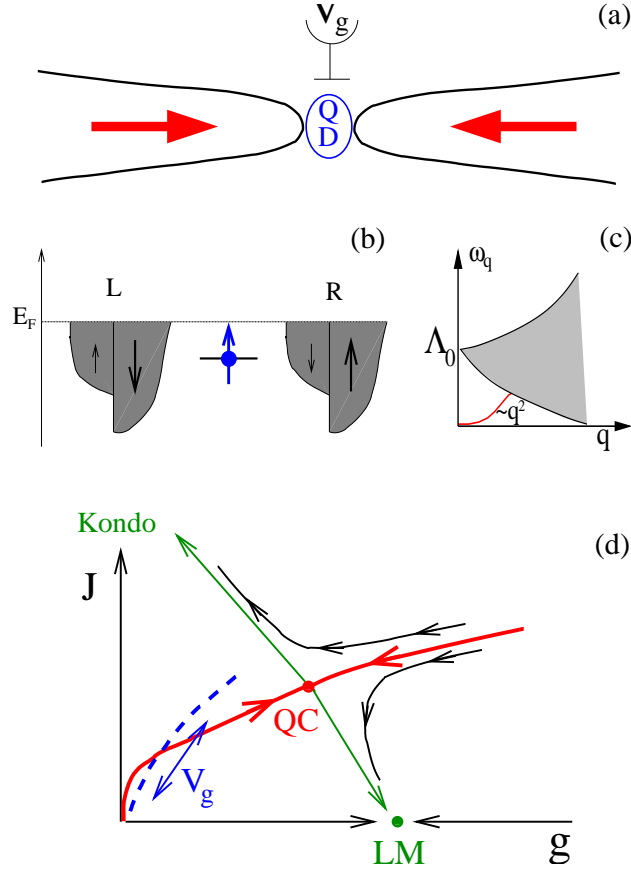


Figure 1: Single-electron transistor with ferromagnetic leads. **a**, A schematic set up. The opposing arrows denote antiparallel (AP) alignment of the magnetizations of the ferromagnetic source and drain.  $V_g$  is the voltage of the normal-metallic gate. “QD” labels the quantum-dot island of a semiconductor quantum dot or a molecule of a single-molecular transistor. **b**, The majority and minority electron bands of the left (“L”) and right (“R”) leads.  $E_F$  labels the Fermi energy. Also shown is the local moment on the dot (blue arrow). **c**, Transverse spin excitations of the ferromagnetic leads. The red line describes spin waves whose energy ( $\omega_{\mathbf{q}}$ ) depends on the wavevector ( $\mathbf{q}$ ) quadratically. The shaded area denotes the continuum associated with particle-hole excitations. The energy of the spin wave at the point it merges into the continuum [ $\Lambda$ , not shown] is of the same order of magnitude as  $\Lambda_0$ , the energy cost to create a particle-hole excitation at  $\mathbf{q} = 0$ . **d**, The phase diagram of the Bose-Fermi Kondo model [see Eq. (9) of the Formal Details section]. The parameters  $J$  and  $g$  are the couplings of the local moment to the fermions and spin waves, respectively. Lines with arrows denote the RG flow. There are three RG fixed points. “Kondo” and “LM” refer to the Kondo screened fixed point, corresponding to a Fermi liquid, and the critical local-moment fixed point, describing a quantum-critical phase. “QC” refers to the quantum-critical fixed point, characterizing the critical Kondo screening on the entire separatrix (red line, corresponding to the critical coupling  $g_c$  as a function of  $J$ ). Varying the gate voltage,  $V_g$ , tunes both  $J$  and  $g$ , along the blue-dashed line.

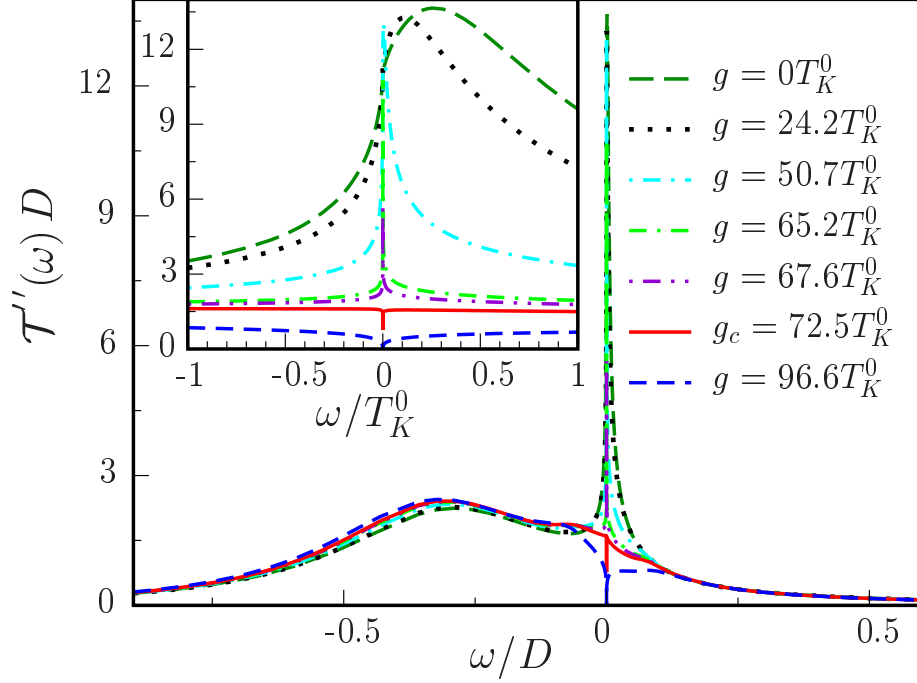


Figure 2: Evolution of the Kondo Resonance. The scattering T-matrix,  $\mathcal{T}(\omega)$ , is defined as the Fourier transform of  $-G_d(\tau) = \langle T_\tau d_\sigma(\tau) d_\sigma^\dagger(0) \rangle$  (where  $\tau$  is the imaginary time) of the Bose-Fermi Anderson model,  $\mathcal{T}''$  is the imaginary part of  $\mathcal{T}$ , and is equal to  $\pi$  times the single-electron spectral function on the dot. The main plot uses the fermionic half-bandwidth,  $D = 1/2\rho_0$ , as the normalization for energies. The peak near  $\omega = 0$ , arising for  $g < g_c$ , corresponds to the Kondo resonance. The inset, limited to the energy range of about  $T_K^0$ , highlights the vicinity of zero energy. Different  $g/T_K^0$  corresponds to different gate-voltage  $V_g$ . The parameters adopted are:  $\epsilon_d = -0.3D$ ,  $U = \infty$ ,  $t = 0.1D$ , corresponding to  $T_K^0 = 4.2 \times 10^{-3}D$ ; the cut-off energy for the bosonic bath [*cf.* Eq. (1)] is  $\Lambda = 0.05D$  and the proportionality factor on the right hand side of Eq. (1) is  $1/\Gamma(3/2)$ . The scaling exponents are universal, but  $g_c/T_K^0$  is not, depending on  $\rho_s$ ,  $\Lambda$  and other microscopic parameters of the ferromagnets. The same parameters apply to Figs. (3,4).

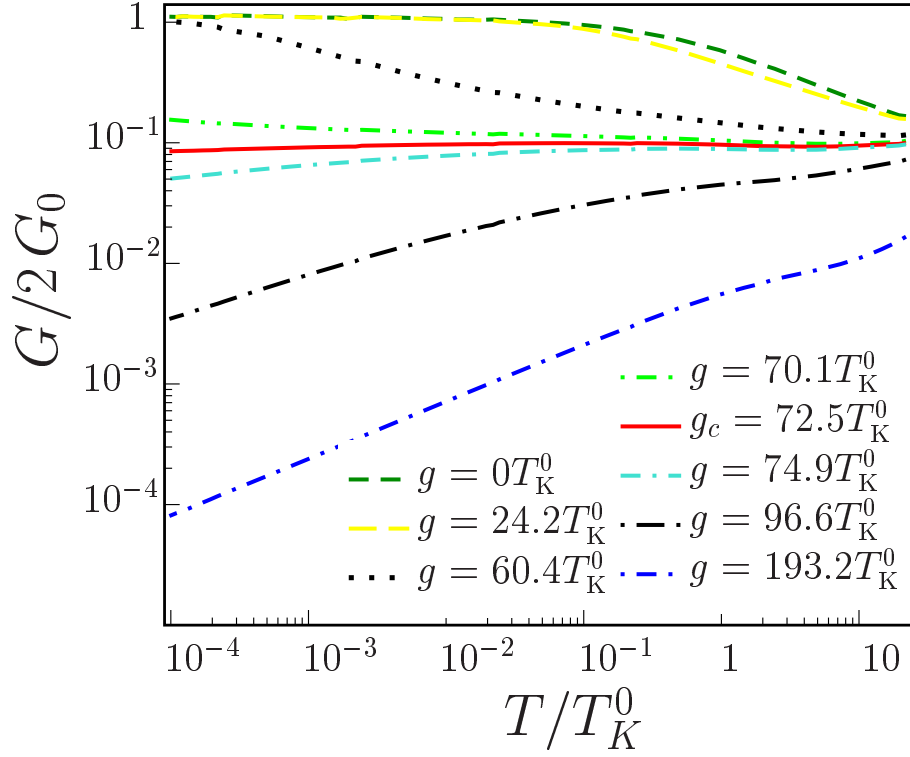


Figure 3: DC conductance. At  $g < g_c$ , the Kondo assisted conductance increases as temperature is lowered. At the QCP ( $g = g_c$ ) and inside the critical local-moment phase ( $g > g_c$ ), the temperature dependence has the forms of Eqs. (2,3), respectively.  $G_0$  is  $e^2/h$ .

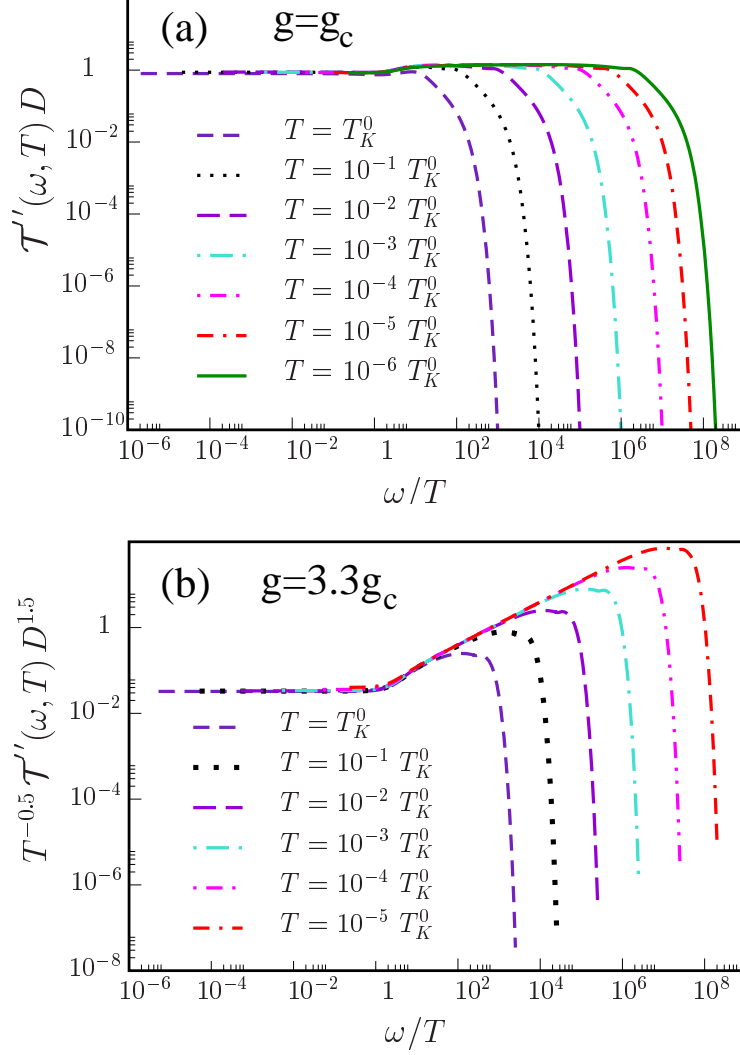


Figure 4:  $\omega/T$  scaling. **a**, The T-matrix as a function of  $\omega/T$ , at the QCP. For each temperature, the T-matrix falls on the universal scaling curve until  $\omega$  reaches the order of  $T_K^0$ . Notice that  $\mathcal{T}''(\omega \rightarrow 0, T \rightarrow 0, \omega/T \rightarrow 0)$  is different from  $\mathcal{T}''(\omega \rightarrow 0, T \rightarrow 0, \omega/T \rightarrow \infty)$ . **b**, Similar result inside the critical local-moment phase, at a  $g > g_c$ ; the critical exponent is 0.5.